arXiv:1610.07678v1 [cond-mat.soft] 24 Oct 2016

Why do magnetic nanoparticles form messy clumps?

N. R. Anderson[a], D. R. Louie[b,*], D. Serantes[a,c,d], K. L. Livesey[a,b]

[a] *UCCS Biofrontiers Center, University of Colorado - Colorado Springs, 1420 Austin Bluffs Parkway, Colorado Springs CO 80918, USA*
[b] *Department of Physics, University of Colorado - Colorado Springs, 1420 Austin Bluffs Parkway, Colorado Springs CO 80918, USA*
[c] *Instituto de Investigacións Tecnolóxicas and Applied Physics Department, Universidade de Santiago de Compostela, 15782 Santiago de Compostela, Spain*
[d] *Department of Physics, University of York, York YO10 5DD, UK*

Abstract

Experiments on magnetic nanoparticles in a viscous medium have shown that agglomerates form that display complex shapes. However, most theoretical results predict more simple, ordered shapes. To account for this discrepancy we have created a theoretical model that phenomenologically includes the interactions between ligands on nearby nanoparticles. Numerical Langevin simulations are performed using ferromagnetic, 50 nm diameter magnetite nanoparticles with a 5 nm thick ligand coating in hexane. The intra-ligand interaction is treated like friction and a unitless parameter c is varied between 0 and 1 to control the strength of the friction. We find that values of c near 0.99 represent a transition from ordered, colinear agglomerates to disordered, noncolinear agglomerates. An analytic estimate for the value of c is provided based on a comparison between the time to diffuse to an agglomerate compared to the time for a nanoparticle to reorient into the local

*Present address: Department of Astronomy, University of Maryland, College Park, MD 20742

magnetic field direction. This estimate also gives a value of c near 0.99, matching the numerical results. Using this model we produce agglomerates that are qualitatively similar to experimental results.

Keywords: magnetic nanoparticle, agglomeration, ferrofluid

1. Introduction

Ferromagnetic and superparamagnetic nanoparticles in liquids are of great interest for a variety of applications including guided drug deliver [1], magnetic hyperthermia (heat) therapy [2], magnetically-tuned liquid crystal displays [3], lab on a chip applications [4], and MRI contrast agents [5]. When the particles are in fluids, there is the possibility for them to agglomerate due to the long-range magnetic dipole-dipole interactions.

Ferromagnetic nanoparticles will form loops to minimize the magnetic dipole-dipole energy in zero field, as long as the magnetic interaction is stronger than thermal fluctuations [6, 7]. In a moderate applied magnetic field, they will instead form single-particle-width chains.[8] These two scenarios are drawn in Fig. 1 in panels (a) and (b). Although this behavior is predicted by many simulations[9, 10], in experiments clumps of particles are far more compact and are more "messy" than simulations predict, as illustrated by the cartoon in Fig. 1(c).[11, 12] Sometimes rather than chains, clumps which are almost isotropic in shape form.[13] Moreover, real agglomerates are often far thicker than those produced through simulation. The question therefore is: why are the experimental clumps so messy?

As an example of the difference between theory and experiment, in Fig. 2 we show the predicted agglomeration (panel a) in comparison with an ex-

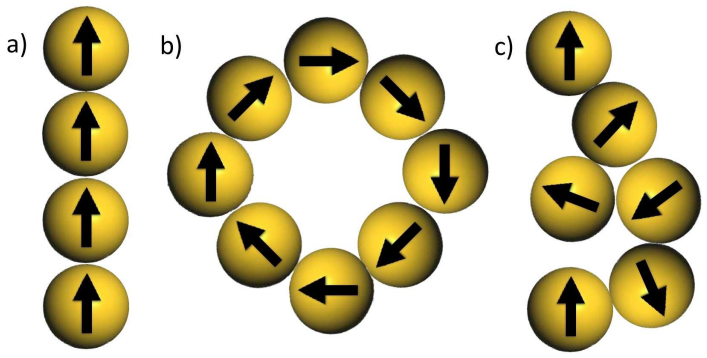

Figure 1: The lowest energy state for dipolar particles in a) a moderate external field, b) in no field, and c) a messy, high-temperature agglomerate of dipolar particles.

perimental result (panel b) in an applied field, taken from Ref. [11]. The simulation parameters used are chosen to match the experiment and are given in the caption. Although the simulation is run with just a few particles to minimize computational time, the contrast in shapes is clear. In panel a), single-width particle chains that are very straight form while in experiment the chains are dendritic and are not straight. Also, some rounded clumps occur that can be seen by the dark, compact blobs that are actually comprised of many particles. (Note that the two chains in panel a) appear to be different sizes due to perspective and the one on the left is in the background.) The details of the simulations will be provided below but this figure is included here to motivate why current Langevin dynamics simulations need to be altered to produce realistic results.

We have performed Langevin dynamics simulations of a small number of single-domain ferromagnetic particles in a liquid using a code built in Fortran, plus using LAMMPS [14], to investigate this question. We characterize the formed agglomerate shapes using normalized length in order to compare the

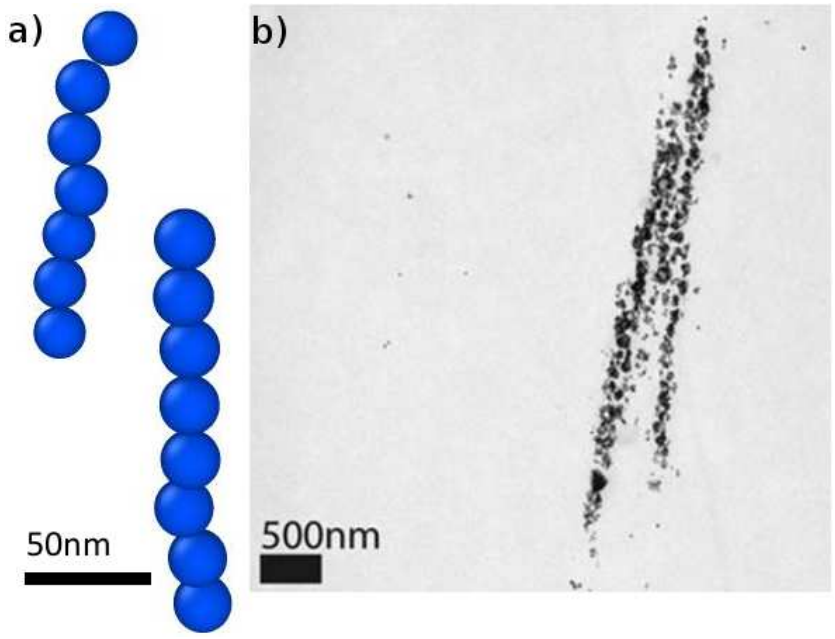

Figure 2: Agglomeration of 22 nm diameter magnetite nanoparticles in water with 5 nm long PEG ligands, and with a 0.27 T applied field, predicted by theory a), and experimentally measured b).[11] Theoretical results predict single particle width agglomerates whereas experimental results show agglomerates with multiple particle widths and messiness even in the presence of an applied field.

simulation results. Introducing thermal buffeting alone does not create the degree of messiness seen in experiment. Nor does a distribution of particle sizes. Instead, we find that if there is *friction* between particles then they may connect in ways that do not minimize the dipole-dipole interaction and that nucleates a clump that will not be a perfect chain, like that seen in Fig. 2(a). The friction must be strong enough so that the timescale for the particles to reorient to minimize their dipole-dipole interaction is longer than the time it takes for another particle to join the clump.

Our hypothesis is consistent with previous simulation results. When mag-

netic nanoparticles are treated as individual bodies without friction between them, then only chains that are one-particle-width form [10]. However, when coarse-graining techniques are used to speed-up simulations – which effectively locks particles together as if friction is infinite – then much thicker and more disordered agglomerates are produced [15]. The "zippering" of chains to form thick chains occurs due to entropic considerations, as discussed by Faraudo *et al.* [16] for large superparamagnetic beads. Furthermore, when particles are forced to remain neighboring (an analogue to introducing friction as we have done), then a variety of agglomerate shapes form depending on the competition between magnetic and thermal energies.[17]

When magnetic nanoparticles form agglomerates, their function is very different compared to isolated particles. For example, MRI contrast is changed [11]. Also, particles may generate more or less heat for magnetic hyperthermia treatment, depending on the cluster shape [13, 18, 19]. As an even simpler example, the clumps may be too large to fit through channels or veins that the individual particles were designed to travel through. It is therefore critically important to know what shape and size particle clumps may have. This work represents a first step in understanding the mechanisms that give rise to realistic shaped agglomerates in that only a small number of particles are simulated to demonstrate that friction is important.

In section 2 we will briefly describe the Langevin dynamics simulation involving single-domain ferromagnetic nanoparticles. We leave it to a later work to consider superparamagnetic particles where the magnetization within a particle may fluctuate as the agglomerate forms. In section 3 we describe the methods used to characterize the particles and the specific parameters

used for the simulations. Then in section 4 we discuss the results and characterize the agglomerate shapes. In section 5 conclusions and future work are presented.

2. Langevin dynamics simulation

The dynamics of each particle i is governed by Newton's second law, expressed as the set of four three-dimensional, first-order, stochastic differential equations. Firstly, we will write these equations without interparticle friction and then describe how they are altered when friction is included. Note that by "friction" we mean the interaction between ligand brushes on particles, not the viscous effect on particles due to the fluid, which is also included in the model. The four equations per particle without friction are:

$$\dot{\vec{x}}(t) = \vec{v}_i(t), \tag{1}$$

$$m_i\dot{\vec{v}}_i(t) = \vec{F}_i\left[\vec{x}_j(t)\right] - m_i\gamma_i\vec{v}_i(t) + \vec{R}_i(t) = \vec{f}_i(t), \tag{2}$$

$$\dot{\theta}_i\hat{u}_i(t) = \vec{\omega}_i(t), \tag{3}$$

$$I_i\dot{\vec{\omega}}_i(t) = \vec{T}_i[\vec{x_j}(t)] - I_i\gamma_i\vec{\omega}_i(t) + \vec{Q}_i(t) = \vec{\tau}_i(t), \tag{4}$$

where the dots over variables indicate time derivatives. Here, $\vec{x}_i(t)$ is the position, $\vec{v}_i(t)$ is the velocity at time t, m_i is the mass of particle i, $\vec{F}_i$ is the total deterministic force acting on the particle due to the other particles (all the contributions to which we will discuss below), γ_i is the viscous coefficient of the particle moving through the fluid, and $\vec{R}_i$ is the random, fluctuating force that describes the effect of finite temperature on the particle. The total force at a time t is $\vec{f}_i(t)$. The angle of rotation is θ_i around the direction $\hat{u}_i$, the angular velocity is $\vec{\omega}_i$, the torque acting on the particle due to the others

is $\vec{T}_i$, the moment of inertia is I_i and the random torque is $\vec{Q}_i$. The total of all torques on particle i at time t is $\vec{\tau}_i(t)$. We will consider identical particles so we can drop the subscript i for the mass m, the moment of inertia I and the viscous friction coefficient γ.

Eqs. (1)-(4) assume that particles may interact but due to thermal fluctuations always have a chance to act individually and escape the forcefield of another, as shown schematically in Fig. 3 on the left. In contrast, assuming that once particles join together (their separation is less than some critical distance) they stay stuck (shown on the right in Fig. 3), is unrealistic as it assumes that particles can never reorient. Instead, we use a model that allows situations between these two extremes. We define a dimensionless friction or stickiness coefficient c_i that is 1 if the particles are stuck together indefinitely and is 0 when particles always act as individual particles. We can then re-write Eqs. (2) and (4) as

$$m_i\dot{\vec{v}}_i(t) = \vec{f}_i(1-c) + \frac{c}{N}\sum_{j=1}^{N}\vec{f}_j, \tag{5}$$

$$I_i\dot{\vec{\omega}}_i(t) = \vec{\tau}_i(1-c) + \frac{c}{N}\sum_{j=1}^{N}\vec{\tau}_j, \tag{6}$$

where the sums are over the N particles that make up an agglomerate that particle i is part of. One can see that if $c = 1$, the agglomerate is treated as a single object, whereas if $c = 0$ a particle is able to move independently, no matter how close it is to others. We will estimate the strength of c in the next section.

We will discuss the viscous and random forces on a particle in more detail before describing the deterministic force contributions to Eq. (2). The drag

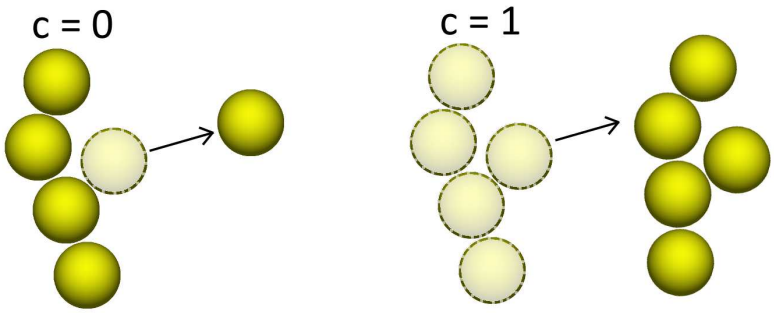

Figure 3: A schematic showing the effect of no interparticle friction ($c = 0$) on the left, and infinite interparticle friction ($c = 1$) on the right.

coefficient in Eq. (2) is given by Stoke's formula [20]

$$m\gamma = 6\pi\eta\mathcal{R}, \tag{7}$$

where η is the viscosity of the fluid and $\mathcal{R}$ is the hydrodynamic radius of the particle. In turn, the viscosity of the fluid is related to the random force of the fluid on a particle $\vec{R}_i(t)$, which is usually assumed to obey a Gaussian distribution centered about zero mean [21, 10]

$$\langle R_\alpha(t)\rangle = 0 \tag{8}$$

$$\langle R_\alpha(t)R_\beta(t+t')\rangle = 6m\gamma k_B T\ \delta_{\alpha\beta}\ \delta(t'), \tag{9}$$

where k_B is Boltzmann's constant, T is temperature, α and β represent the x, y and z components, and $\delta(\tau)$ is the Dirac delta function and $\delta_{\alpha\beta}$ is the Kronecker delta function. Eq. (9) indicates that the random force at time t is completely uncorrelated with the random force at a time t' later. This assumes that the timescales of fluid-particle interactions are much shorter than the characteristic timescales for the particle motion. Similar equations hold for the random torque $\vec{Q}_i(t)$.[10]

The deterministic forces represented by $\vec{F}_i$ in Eq. (2) include steric, van der Waal's and magnetic dipole-dipole and $\vec{T}_i$ are the associated torques. All of these forces depend on the configuration of the particles relative to each other. The van der Waal's attraction force between spherical particles is given by differentiating the energy of interaction [22]

$$V_{Vpp}(\mathcal{D}) = -\frac{A_{131}}{6}\left(\frac{2r^2}{\mathcal{D}^2-4r^2}+\frac{2r^2}{\mathcal{D}^2}+\ln\left(\frac{\mathcal{D}^2-4r^2}{\mathcal{D}^2}\right)\right). \tag{10}$$

Here A_{131} is the Hamaker constant that depends on the material the particles are made from and their shape (in this case spherical), as well as the medium through which they interact. The radius of the particles is r and the center-to-center distance between a pair of particles is $\mathcal{D}$.

The steric repulsive force prevents the ligand-coated particles from overlapping in space. It can be found by differentiating the steric potential between a pair of particles [23]

$$V_{Spp}(\mathcal{D}) = \frac{100rL^3}{(\mathcal{D}-2r)\pi h^3}k_BT\exp\left(-\frac{\pi(\mathcal{D}-2r)}{L}\right), \tag{11}$$

where L is the average length of the ligands, h is the mean distance between two ligand head groups on the surface of the particle, k_B is Boltzmann's constant and T is temperature. Some of these variables are shown in Fig. 4.

The interparticle interactions (van der Waal's and steric) can be added together to create a potential energy curve like the dashed curve shown in Fig. 5 as a function of distance between cores. (We will discuss shortly the parameters used to generate this plot.) It can be seen that there is a minimum energy corresponding to an equilibrium center-to-center separation of roughly 62 nm.

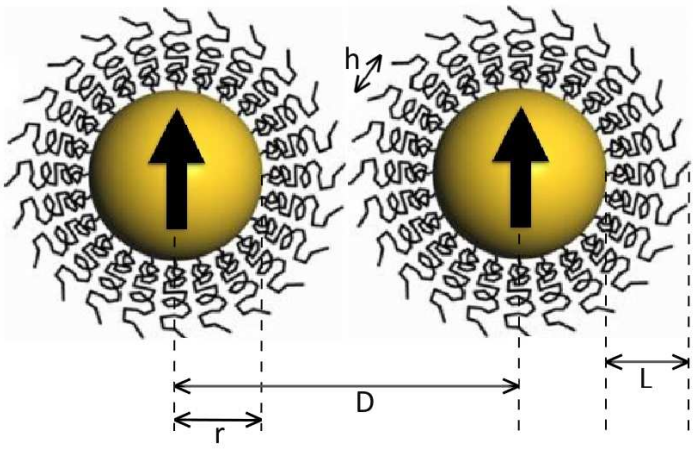

Figure 4: A schematic of two dipolar particles where $\mathcal{D}$ is the interparticle distance, r is the radius of the particle's magnetic core, L is the ligand length and h is the distance between ligand heads.

The solid line in Fig. 5 shows a Lennard-Jones potential fit to the total inter particle interaction. While the Lennard-Jones potential fit doesn't perfectly overlay the steric and Van der Waals potentials, the variation has little effect on the outcome of the numerical simulations. The advantage of using such a fit is that the calculation of forces at each time step of the simulation is vastly simplified for polynomial functions, as compared to exponentials. The Lennard-Jones potential is given by [23]

$$V_{LJ}(\mathcal{D}) = 4\epsilon \left[\left(\frac{\sigma}{\mathcal{D}} \right)^{12} - \left(\frac{\sigma}{\mathcal{D}} \right)^{6} \right], \tag{12}$$

where ϵ is the magnitude of the energy minima (with zero energy given by infinite separation) and σ is the center-to-center separation where the potential crosses zero. We only need to fit Eq. (12) to the interparticle interactions Eqs. (10) and (11) once and then we can use the fit to calculate forces for the forward-time integration.

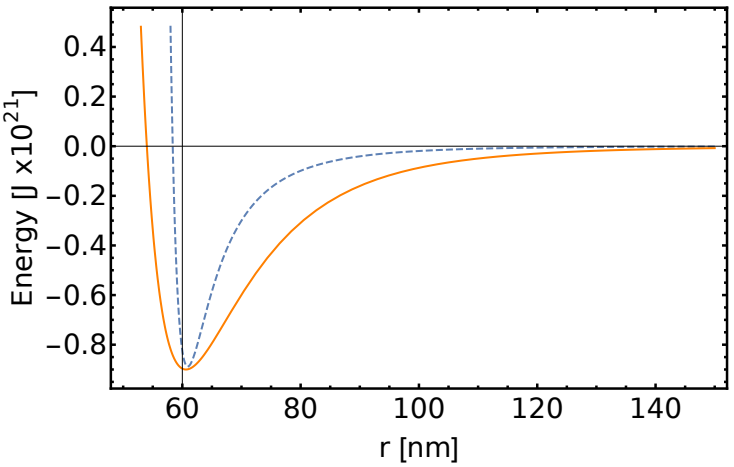

Figure 5: The sum of the Steric and van der Waals potentials for a 50 nm diameter magnetite particle with ligand lengths of 5 nm, a ligand headgroup spacing of 5 nm and a Hamaker constant of 2.9×10^{-20} (dashed line) and a Lennard-Jones fit to the potential with $\sigma = 54$ nm and $\epsilon = 9 \times 10^{-22}$ (solid line).

The final interparticle interaction to be considered is the dipole-dipole interaction. Each particle is assumed to have a magnetic dipole moment given by

$$\vec{m}_i = \vec{M}\frac{4\pi}{3}r^3, \tag{13}$$

where $\vec{M}$ is the saturation magnetization of the material and r is the radius of the nanoparticle. It is assumed that a point dipole located at the center of the particle represents the magnetic properties and so two particles interact via an energy

$$V_{ij}(\vec{r}_i - \vec{r}_j) = -\frac{\mu_0}{4\pi|\vec{r}_i - \vec{r}_j|^3}\left(3(\vec{m}_i \cdot \hat{r}_{ij})(\vec{m}_j \cdot \hat{r}_{ij}) - \vec{m}_i \cdot \vec{m}_j\right), \tag{14}$$

where $\vec{r}_i$ is the position of particle i, the separation between particles is $\mathcal{D} = |\vec{r}_i - \vec{r}_j|$, and $\hat{r}_{ij}$ is a unit vector along the vector $\vec{r}_i - \vec{r}_j$.

The term c models friction between the nanoparticles due to contact of the ligand brushes. While the particles are within a critical distance of each other, namely $\mathcal{D} \leq 2(r + L)$, we apply this friction to all the forces acting on the particles.

There are many numerical routines for solving the equations of motion (1)-(4).[24] We choose to use a modified leap-frog algorithm developed by Van Gunsteren and Berendsen [25]. The random forces (torques) mimicking temperature are converted to random displacements and velocities (rotations and rotational velocities). The reader is referred to the original article for the equations as they are lengthy. The only change we make is the incorporation of the relevant forces for this study and the friction coefficient c.

These algorithms were programmed into Fortran and were tested a number of ways. First, we turn off all forces apart from the viscous and random forces and verify that the equipartition theorem is satisfied. Secondly, we check that the particles acted on only by viscous and random forces should follow "random walk" motion. Thirdly, we compared our results with the frictional parameter $c = 0$ to those calculated using LAMMPS and found agreement. Our fortran code runs at roughly half the speed of LAMMPS code, but has the advantage that our frictional effects characterized by c are included. Both codes are run for just 20 particles and with periodic boundary conditions so that results can be obtained in a reasonable amount of time. It is left to a future work to consider ways to speed up the calculation so that more particles and/or longer times can be simulated.

We have chosen the following parameters for the simulation of magnetite particles with magnetization $M = 3.12 \times 10^5$ A/m, radius $r = 25$ nm, ligand

length $L = 5$ nm, distance between ligand heads $h = 5$ nm and temperature $T = 298$ K. The surrounding fluid is hexane with a viscosity of $\eta = 2.97 \times 10^{-4}$ N s/m^2 and a corresponding Hamaker constant 29×10^{-21} J. [26] The Lennard Jones parameters are $\epsilon = 0.219$ in units of $k_B T$ and $\sigma = 75$ nm. These parameters are chosen such that the sum of dipolar and Lennard Jones energies is at a minimum for a separation distance of 60 nm between the centers of nanoparticles. The timestep throughout the simulation is $\Delta t = 1 \times 10^{-10}$ s and the entire simulation duration is 10 ms. Each simulation consists of 20 particles in a cube with side length 1200 nm using periodic boundary conditions, giving a volume concentration of magnetite of 7.58×10^{-4}.

3. Characterization of agglomerates

To characterize the agglomerate shapes a number of parameters can be used. We have used a normalized length to simply describe the three dimensional shape of agglomerates. The method of calculation for this parameter is given below. Additionally, to compare to experiment other characterization parameters may be of interest. For example the pair correlation function can be calculated [27] and compared to the structure factor which can be experimentally measured. Another quantity of interest is the fractal dimension which can be calculated from a two dimensional image obtained from theory or experiment.[28, 29, 30] Both the pair correlation and fractal dimension gain more value as the number of particles in the system becomes larger and so, we focus on the normalized length.

A particle is identified as part of an agglomerate if it is separated by less than $2(r + L)$ from another particle (see Fig. 4). To calculate the normal-

ized length of an agglomerate we identify the longest axis, defined by the maximum distance between two particles in the agglomerate

$$\mathcal{D}_{\max} = \max_{i,j} \sqrt{(\vec{r}_i - \vec{r}_j)^2}, \tag{15}$$

with i and j indexing all the particles in an agglomerate. The normalized length L_n is then calculated from

$$L_n = \frac{\mathcal{D}_{\max}}{2(r+L)(N_{\text{agg}}-1)}, \tag{16}$$

where N_{agg} is the number of particles in the agglomerate. This length varies from 1, for a two particle agglomerate or a perfectly colinear chain where the particles have no overlap, to a minimum of approximately 0.14. The minimum has been calculated for an arrangement of 20 particles placed in a hexagonal close-packed lattice, where the value $\mathcal{D}_{\max}$ is kept to a minimum and particles cannot overlap. The simulation allows particles to overlap slightly, modeling a meshing of the ligand brushes, which will typically decrease the maximum and minimum values for L_n.

The normalized length is only calculated for the longest chain in the simulation. Initially, $L_n \approx 1$ for all simulations because the number of particles of the first chain is two. For some values of c, agglomerated particles can escape and rejoin the agglomerate or join a different agglomerate. Additionally, when multiple agglomerates form simultaneously the measurement for the normalized length may switch from one agglomerate to another throughout the simulation duration. This adds some "noise" to calculations of L_n and the number of particles agglomerated.

4. Estimates for c and results

In this work we explore the agglomeration behavior of magnetite nanoparticles where the interparticle friction is modeled using the parameter c. Here, we estimate the value of c for which the behavior in the simulations should transition from long chains to clumped agglomerates. We do this by comparing the time it takes a particle to diffuse (t_{diff}) to another, to the time it takes it to rotate so that the magnetic dipolar interactions are minimized ($t_{rotation}$).

A characteristic rotation time for particles in a fluid experiencing a net torque is [31]

$$t_{rotation} \sim \frac{8\pi\eta R_{hyd}^3}{(1-c)\tau_{total}}, \tag{17}$$

where the total torque τ_{total} a particle in an agglomerate experiences is decreased due to friction by the term $(1-c)$, consistent with Eq. (4), and neglecting torques from far away particles (ie. those not in the agglomerate). $R_{hyd} \sim (r+L)$ is the hydrodynamic radius of the particle. This formula comes from the equation for the torque needed to keep a sphere rotating with uniform velocity in a still, infinite, viscous fluid.[32]

This can be compared to the expected time for agglomeration based on the density of particles and the thermal energy. If we assume that the total time t_{total} for a particle to travel to another is equal to the time to diffusively travel to the region close to another particle t_{diff}, plus the time to travel from the near-particle region (defined as where the magnetic interaction energy is equal to the thermal energy) to touching due to magnetic forces t_{mag}, then

we get

$$t_{total} = t_{diff} + t_{mag}. \tag{18}$$

The time for a particle to diffusively travel a distance x is estimated using the fluctuation dissipation theory result as [20]

$$t_{diff} = \frac{x^2 6\pi\eta R_{hyd}}{k_B T}. \tag{19}$$

We estimate x using the mean distance between the 20 particles initially in the simulation volume, minus the distance at which the magnetic interaction overwhelms thermal effects (the near-particle distance $r_{mag} \sim 270$ nm). Therefore we have

$$x = \left(\frac{V}{20}\right)^{1/3} - r_{mag}. \tag{20}$$

Substituting our parameters and Eq. (20) into Eq. (19) finds a diffusion time on the order of 1 ms.

In comparison, the time for a particle to travel from r_{mag} to touching is [31]

$$t_{mag} = \int_{r_{mag}}^{r_{mag}/2} \frac{6\pi\eta R_{hyd}}{F_{magnetic}(r)} dr, \tag{21}$$

where $F_{magnetic}$ is the magnetic force felt by the particles moving together. An estimate using our parameters is that $t_{mag} \sim 0.4$ ms. This means that t_{total} is on the order of 1.4 ms. Note that this is an absolute upper estimate and agrees well with our total simulation time to see all particles agglomerate, which is 10 ms. The estimates do not account for the fact that the first particles have a probability to come into contact more quickly and as soon as one agglomerate nucleates, other particles are drawn towards it reducing

the times. However, the estimates are useful to give analytic dependencies between variables.

When the time for a particle in an agglomerate to rotate so that its magnetic moment points in the local field direction, is larger than the average time for another particle to join the agglomerate, we expect a messy, noncolinear agglomerate to form. The new particle may stabilize the noncolinear shape. One may imagine an incoming particle to have been affected by thermal translations and rotations as well as experiencing the complicated superposition of dipolar fields from all particles on its approach, which is why its magnetic moment is not automatically aligned with the field of the agglomerate it joins. The condition for messy agglomerate shapes is therefore $t_{total} < t_{rotation}$. Rearranging for c and ignoring t_{mag} to simplify the math, one obtains

$$c > 1 - \frac{4k_B T}{3\tau_{total}} \frac{R_{hyd}^2}{x^2}. \tag{22}$$

Then for a given particle concentration and temperature and particle size, we can estimate a friction parameter required to achieve noncolinear agglomerate shapes. Note that for larger thermal energies, less "stickiness" (lower c values) are required for messy clumps to form, as to be expected. Also note here that the fluid viscosity is absent as both t_{rot} and t_{diff} are linearly dependent on viscosity and the term cancels.

Using the above parameters and assuming a magnetic torque τ_{total} for two particles in contact with an angle of 5° between their dipole moments, Eq. (22) gives

$$c > 0.995 \tag{23}$$

for messy agglomerates to form. This value can vary up to $c > 0.999$ by

assuming the angle between dipoles is 90° before they begin to rotate to minimize the dipole-dipole energy.

Therefore, in our Langevin dynamics simulations we expect to find a normalized length of $L_n \approx 1$ for agglomerates when $c < 0.995$ and a decreasing normalized length for increasing values of c. Fig. 6 shows the average normalized length of the largest agglomerate formed after 10 ms as a function of c (on a logarithmic scale), in the absence of an external field. Each data point is calculated using 10 simulations and standard deviations are shown. Above each data point is a picture of a representative agglomerate that was formed in one of the simulations. Small green arrows indicate the direction of each magnetic moment. We see that L_n does not change significantly as c is changed, however the standard deviation is much larger for $c = 0.9$ and $c = 0.0$. This is due to the presence of two quasi-stable states for lower values of c: a ball formed of multiple closed flux loops (the upper agglomerate, small L_n) and a linear chain (the lower agglomerate, large L_n). For values of c closer to 0 the dipole moments tend to align, minimizing the dipolar energy. However, for larger values of c the particles can come in contact with particles that have misaligned dipole moments that become locked in position.

When a field of $\mu_0 H_0 = 0.005$ T is applied (corresponding to an energy $\mu_0 m H_0 = 25 k_B T$) the situation is different. In Fig. 7, we plot again the normalized length as a function of c with each data point being the average of 10 simulations of 10 ms. We see that for values of $c < 0.99$ (less sticky) the agglomerates tend to have $L_n \approx 1$ indicating single-particle-width chains, while for values of $c > 0.99$ (more sticky) the agglomerates have a smaller

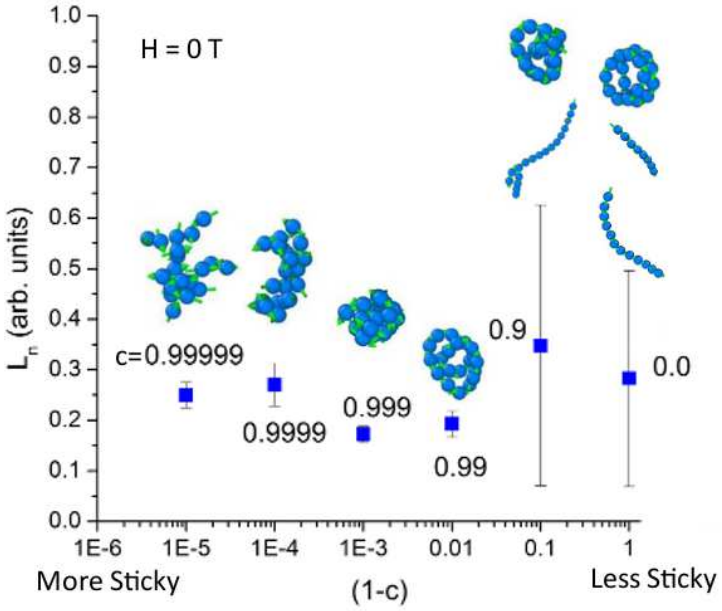

Figure 6: The normalized length L_n versus $(1-c)$ with no applied field, shown on a logarithmic scale. The value of c is displayed and the standard deviation is shown for each value as an error bar. Characteristic agglomerate shapes are also shown for each value of c.

normalized length with $c = 0.99$ being a critical value, as predicted by the estimate in Eq. (22). The critical value is also obvious looking at the representative agglomerates shown on the plot, where for value of $c > 0.99$ messy clumps are formed while for values of $c < 0.99$ linear chains are formed. We also see large standard deviations for values of c around 0.99, again suggesting this is a critical value between colinear chains and "messy" agglomerates. Here the dipole moments tend to align along the field direction, but there is some variation in the alignment for the larger values of c.

The formation of messy agglomerates in an applied field with an energy

of 25 times k_BT is a somewhat surprising result and so we elaborate on the process of agglomerate formation in a field. When c is large, as the particles approach each other the dipole-dipole interaction becomes stronger than the Zeeman interaction at a distance of $\mathcal{D} \approx 93$ nm. Near this distance a particle begins to rotate into the dipole field from the approaching particle. As agglomeration occurs, typically, the particles have not fully rotated into a tip-to-tail orientation, but have a finite angle between both their respective dipole moments and the applied magnetic field. This creates a nucleation site for further noncolinear agglomeration as other particles and agglomerates approach. However, when c is small the same process occurs but after agglomeration the dipole moments continue to rotate into tip-to-tail alignment as well as alignment with the applied magnetic field.

The total duration of the simulations was 10 ms; long enough for all particles to join the agglomerates. But the average time for an agglomerate to form was not the same for all values of c. This is shown for Fig. 8(a) where the number of particles in the largest agglomerate is plotted as a function of time, without an applied field, for different values of c (colored lines). Again, the results are an average of 10 simulations for each value of c. An exponential fit to the simulation data is shown, rather than the data itself, in order to see the trends through the random noise of particles leaving and rejoining the clump. (Representative raw data is shown in the inset to panel (b).) For smaller values of c the particles are not required to remain agglomerated. As such, they sometimes escape from an agglomerate and then later rejoin, keeping the total number of particles in the agglomerate lower. For larger values of c (more sticky) the particles are required to remain attached to

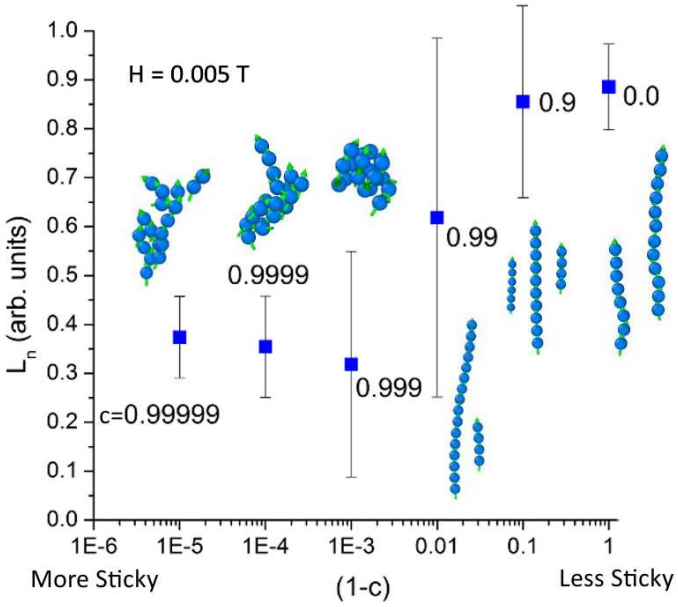

Figure 7: The normalized length L_n versus $(1 - c)$ with a 0.005 T applied field, shown on a logarithmic scale. The value of c is displayed and the standard deviation is shown for each value as an error bar. Characteristic agglomerate shapes are also shown for each value of c.

the agglomerate and so the number of particles in an agglomerate increases faster.

In the presence of an applied field, as in Fig. 8(b), we see different behavior. For small values of c, as the agglomerates form they quickly become short chains aligned with the direction of the field. When these chains are separated along the field axis they attract and form a longer chain, but when they are separated perpendicular to the field axis they repel and remain separate chains. However, when c is large, the agglomerates are not colinear chains and the magnetic fields from the agglomerates tend to attract – on

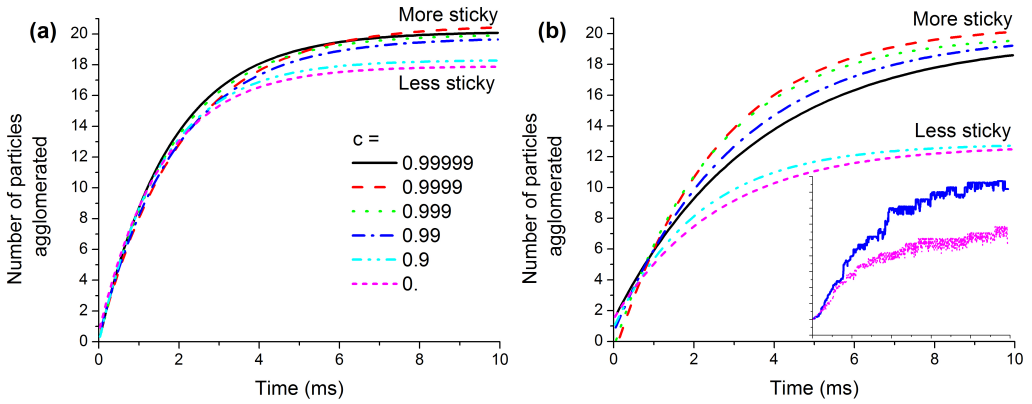

Figure 8: Exponential fits to the number of particles in the largest agglomerate as a function of time, with no applied field a) and a 0.005 T applied field b), for various values of c. The inset in b) shows the raw data for $c = 0.99$ (upper) and $c = 0$ (lower) in a 0.005 T applied field. All fits are done on the average values over 10 simulations.

average – other chains. In the presence of an applied field simulations with larger values of c tend to agglomerate faster.

The "noise" seen in the unsmoothed results (see inset of panel (b) in Fig. 8) is partially due to particles escaping and rejoining the agglomerates, as discussed for smaller values of c, and partially to the way the chain length is calculated through periodic boundaries. The periodic boundaries in our simulations have an interesting effect on larger agglomerates in the absence of an external magnetic field. If two colinear agglomerates come together in a tip-to-tail configuration, due to their significant length with respect to the simulation cube, they would create a dipolar field through the periodic boundaries that encourages colinear chains instead of rings. This behavior can be seen from the large standard deviations in Fig. 6. In this case, even for long total simulation times, the chains never close into loops to have flux

closure. However, when two agglomerates come together in an antiparallel configuration rings are quickly formed. This is the expected outcome[7] for an isolated chain with length greater than ~ 7 particles in the absence of an external field. Increasing the size of our simulation volume would alleviate this problem but would make the system far more dilute and simulations would take significantly longer to do.

The method used to analytically estimate the value of c from Eq. (22) can be extended to look at the behavior of agglomerating systems over a wide range of parameters, whereas we have run simulations of just one particle here. In Fig. 9 we compare the ratio of t_{rot}/t_{total} (scale bar on right) as a function of particle radii and ligand lengths with no friction coefficient ($c = 0$), using a contour plot. Particles in the red (top left) areas of Fig. 9 will form messier agglomerates whereas particles in the pale areas (bottom right) will form linear agglomerates. These results can be easily understood by considering the magnitude of the torque induced by the agglomerate on the considered nanoparticle. When the ligand coating is large (top), the separation between particle centers is larger, decreasing the magnetic torque. Similarly, when the magnetic dipole moments of the particles are small (left) the magnetic torque is again small. In these cases the particles reorient into a tip-to-tail configuration more slowly and noncolinear agglomerates are more likely to be formed. The right side of the graph shows larger radius nanoparticles which approach the multi-domain limit, above which the calculation is no longer valid. The assumptions also break down for particles on the far left side of the graph that are very small and display superparamagnetic behavior.

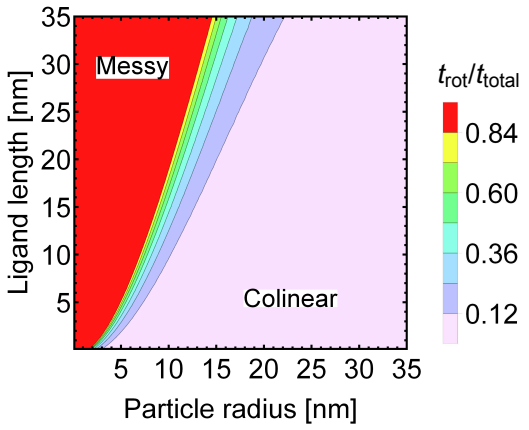

Figure 9: The contour plot shows the ratio of t_{rot} to t_{total} with no friction coefficient ($c = 0$). The legend on the right-hand-side shows what values the colors represent. The red area on the left indicates agglomerates that tend to be messier while the pale area on the right indicate agglomerates that are linear.

5. Conclusion

The torques and forces on touching magnetic nanoparticles due to their ligands can be modeled using a phenomenological stickiness or frictional parameter c. Langevin dynamics calculations with c included indicate a clear transition from linear to clumpy agglomerates forming as a function of c. Additionally, the agglomeration rate is faster when c is larger.

We estimate the critical value of c using a ratio of the diffusion time of a free particle to the rotation time of a magnetic particle in an agglomerate. We find that for values of the stickiness parameter greater than $c = 0.99$, for 50 nm magnetite particles with 5 nm ligand shells, the agglomerates are "messy" but linear chains or loops are formed when c is smaller. This is in complete agreement with our simulation results.

Our calculation should be scaled up to larger volumes, more particles,

and longer times to model real systems. But the fact that we can explain the occurrence of messy agglomerates is of great promise for calculating the properties of real magnetic nanoparticle systems. For example, it has been shown that the shape of agglomerates can dramatically alter the heat produced by magnetic nanoparticles for hyperthermia treatment [13, 18, 19] but the agglomerates so far theoretically studied were all regular shapes (chains, rectangular prisms or spheres). Our simulation results allow for predictions to be made for much more realistic shapes that form in liquids.

Additionally, our calculations for the value of the stickiness coefficient should be compared to physical measurements of the ligand interaction strengths. While specific numbers are lacking for magnetite nanoparticles with PEG ligands, a number of experiments have been done for other surface/ligand combinations including PEG ligands. [33, 34, 35] Among these we find binding forces ranging from 100 - 700 pN over distances from 0 to 7 nm. This gives energies around $10^{19} - 10^{22}$ J which is comparable with the magnetic torques in this analysis. Therefore, the critical value for the stickiness coefficient c that we found seems plausible but needs better experimental validation.

Future work may also add electrostatic interactions to the calculation. This can be done with the same method of incorporating stickiness between touching particles. A screened Coulomb potential can be used and appears to be important for ionic solutions containing magnetite nanoparticles. Recent work has shown that assembly happens at vastly different rates and with different shapes with slight changes in ionic strength.[36]

Acknowledgement

Support is acknowledged from the UCCS Center of the Biofrontiers Institute. D. S. acknowledges financial support from Xunta de Galicia (Spain) under Plan I2C.

References

[1] J. Dobson. Magnetic nanoparticles for drug delivery. *Drug Develop. Res.*, 67(1):55–60, 2006. DOI: 10.1002/ddr.20067

[2] J. P. Fortin, C. Wilhelm, J. Servais, C. Ménager, J. C. Bacri, and F. Gazeau. Size-sorted anionic iron oxide nanomagnets as colloidal mediators for magnetic hyperthermia. *J. Am. Chem. Soc.*, 129(9):2628–2635, 2007. DOI: 10.1021/ja067457e

[3] M. Wang, L. He, S. Zorba and Y. Yin. Magnetically actuated liquid crystals. *Nano Lett.*, 14(7):3966-3971, 2014. DOI: 10.1021/nl501302s

[4] J.-J. Lee, K.-J. Jeong, M. Hashimoto, A. H. Kwon, A. Rwei, S. A. Shankarappa, J. H. Tsui and D. S. Kohane. Synthetic ligand-coated magnetic nanoparticles for microfluidic bacterial separation from blood. *Nano Lett.*, 14(1):1-5, 2014. DOI: 10.1021/nl3047305

[5] B. Bonnemain. Superparamgnetic agents in magnetic resonance imaging: physicochemical characteristics and clinical applications review *J. Drug Target.*, 6(3):167-174, 1998. DOI: 10.3109/10611869808997890

[6] A. Wei, T. Kasama and R. E. Dunin-Borkowski. Self-assembly and flux closure studies of magnetic nanoparticle rings. *J. Mater. Chem.* 21:16686-16693, 2011. DOI: 10.1039/C1JM11916H

[7] P. Jund, S. G. Kim, D. Tománek and J. Hetherington. Stability and Fragmentation of Complex Structures in Ferrofluids. *Phys. Rev. Lett.*, 74, 3049, 1995. DOI: https://doi.org/10.1103/PhysRevLett.74.3049

[8] G. Cheng, D. Romero, G. T. Fraser and A. R. H. Walker. Magnetic-field-induced assemblies of cobalt nanoparticles. *Langmuir*, 21(26):12055-12059, 2005. DOI: 10.1021/la0506473

[9] L. Rovigatti, S. Kantorovich, A. O. Ivanov, J. M. Tavares, and F. Sciortino. Branching points in the low-temperature dipolar hard sphere fluid. *J. Chem. Phys.*, 139(13):134901, 2013. DOI: http://dx.doi.org/10.1063/1.4821935

[10] Z. Wang, C. Holm and H. W. Müller. Molecular dynamics study on the equilibrium magnetization properties and structure of ferrofluids. *Phys. Rev. E*, 66:021405, 2002. DOI: https://doi.org/10.1103/PhysRevE.66.021405

[11] S. L. Saville, R. C. Woodward, M. J. House, A. Tokarev, J. Hammers, B. Qi, J. Shaw, M. Saunders, R. R. Varsani, T. G. St Pierre, and O. T. Mefford. The effect of magnetically induced linear aggregates on proton transverse relaxation rates of aqueous suspensions of polymer coated magnetic nanoparticles. *Nanoscale*, 5:2152–2163, 2013. DOI: 10.1039/c3nr32979h

[12] C. Martinez-Boubeta, K. Simeonidis, D. Serantes, I. Conde-Leborán, I. Kazakis, G. Stefanou, L. Peña, R. Galceran, L. Balcells, C. Monty, D. Baldomir, M. Mitrakas, and M. Angelakeris. Adjustable Hyperthermia Response of Self- Assembled Ferromagnetic Fe-MgO Core-Shell Nanoparticles by Tuning Dipole-Dipole Interactions. *Adv. Funct. Mater.*, 22(17):37373744, 2012. DOI: 10.1002/adfm.201200307

[13] S. L. Saville, B. Qi, J. Baker, R. Stone, R. E. Camley, K. L. Livesey, L. Ye, T. M. Crawford, and O. T. Mefford. The formation of linear aggregates in magnetic hyperthermia: Implications on specific absorption rate and magnetic anisotropy. *J. Colloid Interf. Sci.*, 424:141–151, 2014. DOI: 10.1016/j.jcis.2014.03.007

[14] S. Plimpton. Fast parallel algorithms for short-range molecular dynamics. *J. Comp. Phys.*, 117:1-19, 1995. www.lammps.sandia.gov. DOI: 10.1006/jcph.1995.1039

[15] A. Satoh, R. W. Chantrell, S.-I. Kamiyama and G. N. Coverdale. Two-dimensional Monte Carlo simulations to capture thick chainlike clusters of ferromagnetic particles in colloidal dispersions. *J. Colloid Interf. Sci.*, 178:620-627, 1996. DOI: 10.1006/jcis.1996.0159

[16] J. Faraudo, J. S. Andreu, C. Dalero and J. Camacho. Predicting the self-assembly of superparamagnetic colloids under magnetic fields. *Adv. Funct. Mater.*, 2016. DOI:10.1002/adfm.201504839

[17] A. F. Pshenichnikov and A. A. Kuznetsov. Self-organization of magnetic moments in dipolar chains with restricted de-

grees of freedom. *Phys. Rev. E*, 92(4):042303, 2015. DOI: https://doi.org/10.1103/PhysRevE.92.042303

[18] D. Serantes, K. Simeonidis, M. Angelakeris, O. Chubykalo-Fesenko, M. Marciello, M. del Puerto Morales, D. Baldomir, and C. Martinez-Boubeta. Multiplying magnetic hyperthermia response by nanoparticle assembling. *J. Phys. Chem. C*, 118(11):5927–5934, 2014. DOI: 10.1021/jp410717m

[19] R. P. Tan, J. Carrey, and M. Respaud. Magnetic hyperthermia properties of nanoparticles inside lysosomes using kinetic Monte Carlo simulations: Influence of key parameters and dipolar interactions, and evidence for strong spatial variation of heating power. *Phys. Rev. B*, 90:214421, 2014. DOI: https://doi.org/10.1103/PhysRevB.90.214421

[20] R. K. Pathria and P. D. Beale, *Statistical Mechanics, Third Edition* (Elsevier, Oxford, 2011).

[21] R. Kubo. The fluctuation-dissipation theorem. *Rep. Prog. Phys.* **29**, 255-284, 1966. DOI: 10.1088/0034-4885/29/1/306

[22] H. C. Hamaker. The London-van der Waals attraction between spherical particles. *Physica*, 4(10):1058–1072, 1937. DOI: http://dx.doi.org/10.1016/S0031-8914(37)80203-7

[23] J. N. Israelachvili. *Intermolecular and Surface Forces, Third Edition* (Elsevier, Waltham, 2011). ISBN: 978-0123919274

[24] M. P. Allen and D. J. Tildesley. *Computer Simulation of Liquids* (Clarendon Press, Oxford, 1987). ISBN: 978-0198556459

[25] W. F. Van Gunsteren and H. J. C. Berendsen. A Leap-frog Algorithm for Stochastic Dynamics. Mol. Simul. **1**, 173-185, 1988. DOI: http://dx.doi.org/10.1080/08927028808080941

[26] B. Faure, G. Salazar-Alvarez, and L. Bergstrom. Hamaker constant of iron oxide nanoparticles. *Langmuir* 27(14): 8659-8664, 2011. DOI: 10.1021/la201387d

[27] J. García-Otero, M. Porto, J. Rivas and A. Bunde. Influence of dipolar interaction on magnetic properties of ultrafine ferromagnetic particles. *Phys. Rev. Lett.*, 84(1):167-170, 2000. DOI: 10.1103/PhysRevLett.84.167

[28] M. Wozniak, F. R. A. Onofri, S. Barbosa, J. Yon, and J. Mroczka. Comparison of methods to derive morphological parameters of multifractal samples of particle aggregates from TEM images. *J. Aerosol Sci.*, 47:12–26, 2012. DOI: http://dx.doi.org/10.1016/j.jaerosci.2011.12.008

[29] J. Liu, Z. Wang, A. Sheng, F. Liu, F. Qin, and Z. L. Wang. In situ observation of hematite nanoparticle aggregates using liquid cell transmission electron microscopy. *Environ. Sci. Technol.*, 50(11):5606-5613, 2016. DOI: 10.1021/acs.est.5b06305

[30] J. Teichmann and K. G. van den Boogaart. Cluster models for random particle aggregates – morphological statistics and collison distance. *Spat. Stat.*, 12:65-80, 2015. DOI: http://dx.doi.org/10.1016/j.spasta.2015.03.002

[31] D. V. Berkov, N. L. Gorn, R. Schmitz and D. Stock. Langevin dynamic simulations of fast remagnetization processes in ferrofluids with internal magnetic degrees of freedom. *J. Phys.-Cond. Mat.*, 18:S2595, 2006. DOI: http://dx.doi.org/10.1088/0953-8984/18/38/S05

[32] H. Lamb, *Hydrodynamics* (Dover, New York, 1945), p. 589.

[33] S. Sun, G. Zhao, Y. Huang, M. Cai, Y. Shan, H. Wang and Y. Chen. Specificity and mechanism of action of alpha-helical membrane-active peptides interacting with model and biological membranes by single-molecule force spectroscopy. *Sci. Rep.* 6:29145, 2016. DOI: 10.1038/srep29145

[34] Y. Xue, X. Li, H. Li, and W. Zhang. Quantifying thiol-gold interactions towards the efficient strength control. *Nat. Commun.* 5:4348, 2014. DOI: 10.1038/ncomms5348

[35] M. Dong and O. Sahin. A nanomechanical interface to rapid single-molecule interactions. *Nat. Commun.* 2:247, 2011. DOI: 10.1038/ncomms1246

[36] L. Ye, T. Pearson, Y. Cordeau, O. T. Mefford, and T. M. Crawford. Triggered self-assembly of magnetic nanoparticles. *Sci. Rep.*, 26:3983-3989, 2016. DOI: 10.1038/srep23145